Journal of Sound and Vibration 326 (2009) 190–204

Contents lists available at ScienceDirect

Journal of Sound and Vibration

journal homepage: www.elsevier.com/locate/jsvi

Characterization of impervious layers using scale models and an inverse method

J. Alba [a], E. Escuder [a,*], J. Ramis [b], R. Del Rey [a]

[a] Department of Applied Physics, Higher Polytechnical School of Gandia, Polytechnical University of Valencia, Ctra Nazaret-Oliva s/n, 46730 Gandia, Spain
[b] Department of Physics, Engineering of Systems and Theory, University of Alicante, Zip code 99, 03080 Alicante, Spain

ARTICLE INFO

Article history:
Received 6 March 2008
Received in revised form
22 April 2009
Accepted 29 April 2009
Handling Editor: C.L. Morfey
Available online 9 June 2009

ABSTRACT

We describe a novel procedure that uses an inverse method to determine unknown parameters for impervious layers used in multilayer structures. The proposed model of the multilayer structure is limited to an ideal double plate separated by an unbonded, fibrous, sound-absorbing material. Experimental data were obtained by nearfield acoustic holography for the calculation of the transmission loss of various multilayer structures mounted in a window in a wooden box designed specifically for this purpose. We used the Trochidis and Kalaroutis forecast model of acoustic insulation for multilayer structures, which is based on a spatial Fourier transform. The experimental pressure and velocity data were used as input data in the inverse method. By applying the Trochidis and Kalaroutis model and using numerical methods to adjust the variables that define the impervious layers of the system, the values of the unknown parameters of the layers could then be calculated. For validation, the results were compared with results obtained using the Ookura and Saito model, based on impedance coupling between layers and using the statistical-energy-analysis model, which subdivides the system into subsystems. We evaluate the measurement errors associated with the construction of a hologram by nearfield acoustic holography, i.e., errors due to sensor mismatch and position mismatch, in terms of their probabilities.

1. Introduction

Various theories are used to describe the acoustic behaviour of multilayer structures, including the Ookura and Saito model [1], based on impedance coupling between layers; the Trochidis and Kalaroutis [2] and Bruneau [3] models, based on a spatial Fourier transform (SFT); the theory of Lauriks et al. [4], based on Biot's theory; the theory of Crocker and Price, based on the statistical-energy-analysis (SEA) model [5]; and the theory of Panneton and Atalla, based on finite element methods [6]. Trochidis and Kalaroutis developed a method in which a matrix is obtained that defines a multilayer structure [2]. This model is based on boundary conditions between the layers, yielding various equations with partial derivatives that can be transformed into algebraic equations using a spatial Fourier transform. These algebraic equations can then be solved, providing information about the acoustic variables of the multilayer structure. The model of Ookura and Saito analyses the sound transmission index for a multilayer structure by impedance transfer for inclined-incident-angle waves and random sound fields [1]. The SEA model divides a complex built-up structure into a number of subsystems. From an

* Corresponding author. Tel.: +34 96 284 93 14; fax: +34 96 284 93 09.
E-mail address: evescude@fis.upv.es (E. Escuder).

0022-460X/$ - see front matter © 2009 Elsevier Ltd. All rights reserved.
doi:10.1016/j.jsv.2009.04.045

energy balance, based on the energy exchange between the subsystems and the energy dissipation within the subsystems, an overall vibration response can be obtained for each subsystem [7].

Most models are based on two types of structural materials: sound-impervious materials and sound-absorbing materials. For sound-absorbing materials such as mineral or organic wool, textile or glass fibre and open honeycomb-like layers, a small portion of the incident sound is reflected. The air particles that penetrate through the material continue to vibrate, causing friction against the walls of pores, which leads to a reduction in the kinetic energy of the particle velocity via a friction-related transformation into thermal energy [8]. The absorption depends on the frequency and angle of the incident sound wave. Sound propagation through sound-absorbing materials is usually characterized, in the case of homogeneous, isotropic materials, by two complex values that depend on the sound frequency: a complex propagation constant (Γ) and a complex characteristic impedance (Z) [9]. Other methods can also be used to characterize sound-absorbing materials, for example the Kundt impedance tube [10,11]; many such methods are described in the literature [9,12,13].

A material is considered to be impervious to sound if the pressure wave is unable to enter its interior. Such materials are characterized by the fact that when an incident sound wave is present, the material acquires a vibration velocity, radiating acoustic energy from the opposite face. Physically, no pressure wave crosses the material; instead, an incident wave generates a vibration velocity that generates a transmitted pressure wave (air noise). Sound-impervious layers reflect most of the energy of the wave. The acoustic wave causes vibration of a plate of the material and the acoustic field inside the layer is characterized by a certain vibration velocity [1,2].

A thin, plane, uniform surface with a given rigidity is assumed; it vibrates with a small displacement amplitude. This thin plate is characterized by a surface density m (in units of kg/m^2) and a given rigidity [14]. Within the plate, the restoring force is governed only by its rigidity. The general equation that governs the movement for symmetrical vibrations is as follows:

$$\nabla^4 w(x,y,t) + \frac{\rho(1-\sigma^2)}{Yh^2}\frac{\partial^2 w(x,y,t)}{\partial t^2} = 0 \tag{1}$$

where ρ (kg/m^3) is the volume density of the material, σ the Poisson coefficient, Y (N/m^2) the Young's modulus and h (m) the radius of curvature of the surface, which has a value given by $h = L/\sqrt{[]}12$, where L is the thickness of the plate. Eq. (1) can also be expressed as follows:

$$D\nabla^4 w(x,y,t) + \rho L\frac{\partial^2 w(x,y,t)}{\partial t^2} = 0 \tag{2}$$

where D (N m) is the flexural rigidity of the plate, given by

$$D = \frac{YL^3}{12(1-\sigma^2)} \tag{3}$$

A number of mathematical models have been developed to estimate the relationship between the transmitted and incident pressure waves, i.e., to estimate the coefficient of sound transmission of the impervious material or a layer of it. These models generally require accurate data on the elastic properties of the material, as this is the most important factor in terms of vibration velocity. The surface density also affects transmission coefficients at low frequencies. Models that take account of this effect also require values for the flexural stiffness (D), surface density (ρ), thickness (h) and loss factor (η) of the layer [15].

Inverse analysis normally refers to the parameters of a system that provide the best fit between the calculated and observed acoustic behaviour. Inverse analysis is more complex than direct analysis, as the mathematical problem consists of the minimization of a nonlinear function. This function is an error function that is calculated as the difference between the calculated and measured data using a given combination of parameters. Such techniques are useful because the calculated parameters can be used in making estimates for future stages of the same project, thereby minimizing potential inaccuracies in the model employed [16,17]. Various studies have made use of inverse methods for determining material properties based on finite element analysis and modal analysis [18–20].

In the present paper, we use an inverse method to determine unknown parameters for multilayer structures, using values obtained from nearfield acoustic holography (NAH) as input data and the multilayer prediction model described above. The NAH technique is based on a measurement of the amplitude and phase of the sound pressure using an array microphone positioned in a plane that is both parallel and close to the measurement area. Using digital data-processing techniques, NAH values can be used to calculate acoustic magnitudes on the object surface by back-propagation of the acoustic field. The main advantage of NAH is that the sound field in any other plane of the object can be reconstructed from 2-D values; this reconstructed sound field is termed a hologram [21–25]. There exist various sources of measurement error associated with the construction of a hologram by NAH, namely errors due to sensor mismatch and position mismatch. We have studied these errors in terms of their probabilities, bias and random errors [26]. This approach can be used in practical applications because the theoretical models used are normally applied to ideal partitions with elastic properties that do not

vary with the incidence angle of the sound wave. Therefore, complementary calculation techniques can be used to ensure the optimal application of the theoretical models to real structures, with no need for real-time measurements.

2. Fundamentals

2.1. The inverse method

Once the values of the parameters that characterize the layers and sound-absorbing material of a system are known, the Trochidis and Kalaroutis model can be used to estimate the transmission loss (TL) in the multilayer structure. In an inverse model, the values of the experimental transmission loss can be used to obtain the system parameters that achieve the best fit between the theoretical and experimental results.

The inverse method for the identification of parameters is based on iterative loops between the experimental data and the prediction model, using several different values of the parameters of the structural materials to optimize the results and minimize the model error. To this end, we use an error function that has a minimum value for the most suitable parameters of the plates (Fig. 1).

Parameter identification techniques are used to obtain the parameters of the model that provide the best fit between the real-time measurements and the model predictions. The problem of estimating parameters using real-time measurements can be solved by using an explicitly formulated model that relates a number of measurements x to a certain number of parameters of which we have no *a priori* knowledge:

$$\mathbf{x} = \mathbf{Z}(\mathbf{y}) \tag{4}$$

where $\mathbf{Z}$ represents the model. The relation expressed by $\mathbf{Z}$ is nonlinear. The inverse problem consists of finding a set of parameters $\mathbf{y}$ such that the variables $\hat{x}_i$ calculated using those parameters via Eq. (4) provide a better fit to the real-time measurements x_i.

Data fitting is performed mathematically on the basis of an identification criterion. The selection of the criterion determines the function whose maximum and minimum correspond to the solution of the problem. There are several different identification criteria, but the most widely used are the least-squares and maximum-likelihood criteria. Each criterion requires a certain level of initial information; criteria with a greater degree of generality require larger amounts of information. In the present study, we used the mean square error function, expressed as follows:

$$\varepsilon = \sum_{i=1}^{n} (\tau_i - \hat{\tau}_i)^2 \tag{5}$$

where τ_i represents the value of the transmission coefficient obtained from experimental measurements at frequency i ($\tau_i = I_t/I_{\text{in}}$, where I_t is the transmitted intensity and I_{in} the incident intensity) and $\hat{\tau}_i$ the theoretical value given by the model. In this case, ε is dimensionless because τ_i and $\hat{\tau}_i$ are dimensionless.

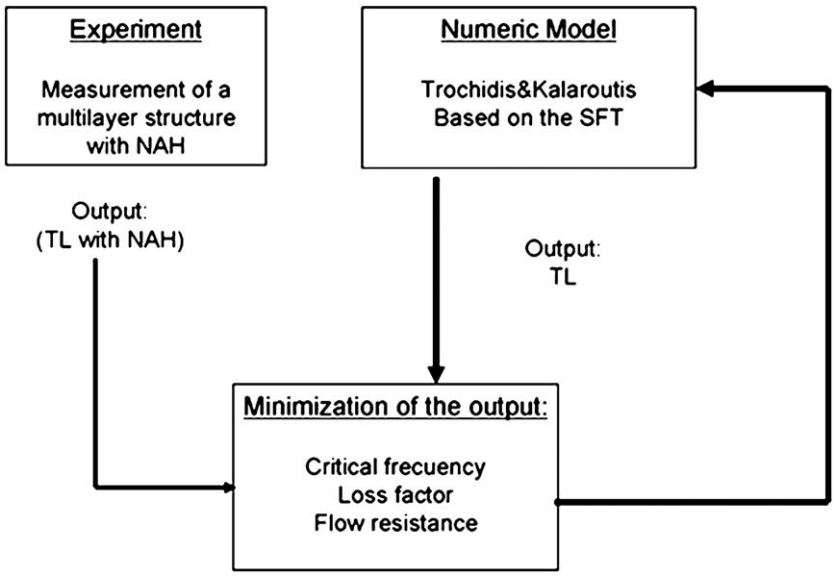

Fig. 1. Diagram of the inverse method.

The steps to be followed in the minimization process are as follows:

- the iterative process starts with an initial approximation y_0 and
- the next approximation to the solution adds an increment to the initial approximation:

$$y_{k+1} = y_k + \Delta y_k \tag{6}$$

We proceed in this way until convergence is achieved. A convergence criterion is applied to the derivative of the error function; we search for the zero value of the derivative, which coincides with a maximum or minimum value. Convergence can impose demanding conditions such as $\|\Delta y_k\| < \varepsilon$, i.e., the modulus of the increment of the approximation to the parameters obtained using this method is small and the function barely varies, because an exact solution of the problem is not usually obtained by numerical methods. Both of the above conditions must be simultaneously fulfilled, because when the increment of the approximation generates a significant reduction in the error function, the iterative process must continue until the function is minimized [27,28].

The model was adjusted to the characteristics of the materials. The model used three variables:

- The surface density, which was measured. The refinement with respect to the initial value was small, affecting only the last decimal, which did not cause the value obtained for the isolation to change.
- Measurements of the Young's modulus and shear modulus were carried out by ultrasound and the results were similar to the input data. The refinement was again small.
- The loss factor is a parameter that depends on the frequency; in the model, a constant total loss factor was used. That is to say, the model, which is an accepted model, simplifies the loss factor to a constant value. This parameter depends on the internal loss factor, on the irradiation factor of the material and on the conditions of fixation. In our case, we tried to diminish the effect of the conditions of fixation by means of elastic elements for support. An average value was obtained with this method that we considered to be valid for the range of frequencies used, considering the tolerance that already exists in this type of measurement [29].

2.2. Trochidis and Kalaroutis model based on a spatial Fourier transform

This theoretical model consists of two infinite, thin, elastic plates with no connection between them. A sound-absorbing material is placed between them [2] in such a way that a gap exists between the plates and the intervening material (Fig. 2).

The multilayer structure is excited with a plane wavefront that is incident on the structure at an angle θ from the direction normal to the structure. The time dependence is assumed to be $e^{-j\omega t}$, where ω is the angular frequency. Zones I, II, IV and V are described by a Helmholtz scalar equation, representing the propagation of sound in air:

$$[\nabla^2 + k_0^2]p_i(x,z) = 0, \quad i = \mathrm{I, II, IV, V} \tag{7}$$

where $k_0 = \omega/c_0$ is the wavenumber of the sound.

The equation that describes the movement of Plate I can be expressed as

$$[D_1\nabla^4 - \rho_1 h_1 \omega^2]w_1(x) = p_{\mathrm{I}}(x,0) - p_{\mathrm{II}}(x,0) \tag{8}$$

where $w_1(x)$ is the plate displacement in the normal direction, ρ_1 the density of the plate material, h_1 the thickness of the plate, D_1 the flexural stiffness of the plate and $p_{\mathrm{I}}(x,z)$ and $p_{\mathrm{II}}(x,z)$ are the sound pressures in Zones I and II, respectively. The space filled with the sound-absorbing material (Zone III) is represented by a complex wavenumber k_b and a complex

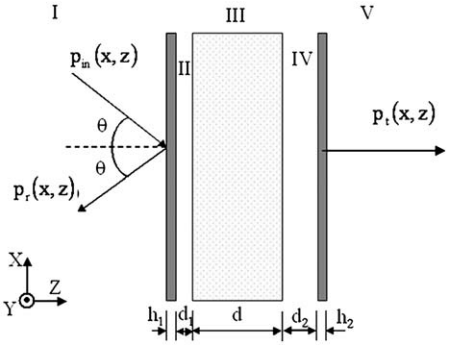

Fig. 2. Multilayer model under study.

density ρ_b. The wave equation for the sound-absorbing material is as follows:

$$[\nabla^2 + k_b^2]p_{\mathrm{III}}(x,z) = 0, \quad h_1 + d_1 < z < d + h_1 + d_1 \tag{9}$$

The equation that describes the movement of the outer plate, Plate II, is

$$[D_2\nabla^4 - \rho_2 h_2 \omega^2]w_2(x) = -p_{\mathrm{V}}(x, d + h_1 + d_1 + h_2 + d_2) + p_{\mathrm{IV}}(x, d + d_1 + h_1 + d_2) \tag{10}$$

where $p_{\mathrm{IV}}(x,z)$ is the sound pressure in Zone IV (air) and $p_{\mathrm{V}}(x,z)$ the sound pressure in Zone V.

This method generates a matrix for the multilayer structure, which is obtained by directly applying the boundary conditions for the materials. This results in various equations with partial derivatives that can be transformed into algebraic equations via an SFT. The algebraic equations are then solved, providing information on the acoustic variables of the multilayer structure.

Once the transmitted sound pressure $p_t(x,z)$ is known, the transmission coefficient for a wave incident at an angle θ can be calculated from [1]

$$\tau(\theta) = \left|\frac{p_t}{p_{\mathrm{in}}}\right|^2 \tag{11}$$

If the incident pressure field fulfils the conditions of a diffuse field, which is what happens in actual cases, the transmission coefficient can be obtained from

$$\tau_d = \frac{\int_0^{\theta_{\mathrm{lim}}} \tau(\theta)\cos\theta\sin\theta\,\mathrm{d}\theta}{\int_0^{\theta_{\mathrm{lim}}} \cos\theta\sin\theta\,\mathrm{d}\theta} \tag{12}$$

where θ_{lim} represents the limit angle at which any contribution to the sound field is negligible. From Eq. (9), the transmission loss can be obtained from the following expression:

$$\mathrm{TL} = -10\log\tau_d \tag{13}$$

The mean square error function is $\varepsilon = \sum_{i=1}^{n}(\mathrm{TL}_i - \hat{\mathrm{TL}}_i)^2$, where TL_i represents the value of the transmission loss obtained from the experimental measurements at frequency i and $\hat{\mathrm{TL}}_i$ is the theoretical value derived from the model. ε is expressed in dB because TL_i and $\hat{\mathrm{TL}}_i$ are also measured in dB.

2.3. Nearfield acoustic holography

The acoustic field of any monochromatic source can be decomposed into an angular spectrum that is defined in the wavenumber domain as a superposition of plane waves travelling in different directions; however, not all of the waves are propagated in the normal way: some decay exponentially with increasing distance. Nearfield acoustic holography is a technique that reconstructs the sound field and vibration velocity of an object or sound source from measurements taken with microphones placed in a plane that is both parallel to and close to the sound source (see Fig. 3). The nearfield measurements enable the capture of the evanescent waves (subsonic waves that decay exponentially with increasing distance from the sound source) that are generated by the sound source and which contain high-resolution details about

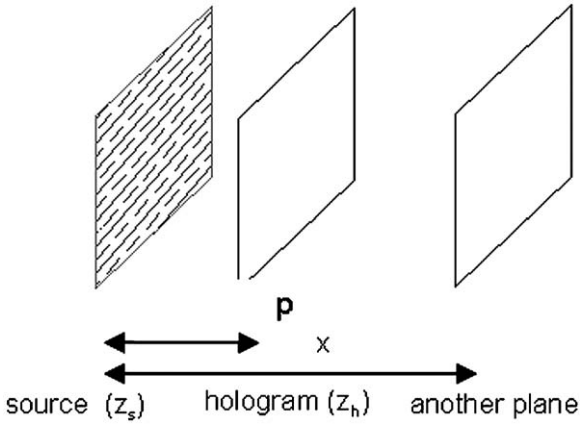

Fig. 3. Three measurement planes.

the source [30,31]. NAH involves the measurement of the amplitude and phase of the sound pressure using a flat array microphone.

Based on Green's theorem, an integral can be derived that describes the sound pressure at any point in space between the sound source and the measurement plane. The complex pressure at any point in free space can be expressed as a function of the complex pressure ($\bar{p}$) in the source plane z_s, where $\bar{p}_s(x',y',z_s)$ is the distribution of the complex pressure on z_s and $\bar{G}'(x-x',y-y',z-z_s)$ is the normal derivative of the Green's function that satisfies the Dirichlet eigenvalue limit condition on z_s [32]:

$$\bar{p}(x,y,z) = -\int_{-\infty}^{\infty}\int \bar{p}_s(x',y',z_s)\times \bar{G}'(x-x',y-y',z-z_s)\,\mathrm{d}x'\,\mathrm{d}y' \tag{14}$$

If all points are assumed to be located in the same measurement plane, termed the hologram plane, z_h, the above equation becomes

$$\bar{p}_h(x,y,z_h) = \int_{-\infty}^{\infty}\int \bar{p}_s(x',y',z_s)\times \bar{G}'(x-x',y-y',z_h-z_s)\,\mathrm{d}x'\,\mathrm{d}y' \tag{15}$$

As z_h–z_s is a constant, Eq. (15) describes a 2-D convolution between the complex pressure in the plane z_s and the modified Green's function, which becomes a simple product in the wavenumber domain:

$$\bar{p}_h(k_x,k_y,z_h) = \bar{p}_s(k_x,k_y,z_s)\cdot \bar{G}'(k_x,k_y,z_h-z_s) \tag{16}$$

where z_h–z_s is defined as the distance between the source plane and the hologram plane. Once the sound pressure $\bar{p}(k_x,k_y,z_h)$ is known in the space of k, the particle velocity vector can be determined by applying the Euler equation, considering the harmonic acoustic fields in the time domain and applying the inverse Fourier transform:

$$\bar{v}(k_x,k_y,z) = \frac{1}{\omega\rho}\left(k_x e_x + k_y e_y - \mathrm{i}e_z\frac{\partial}{\partial z}\right)\bar{p}(k_x,k_y,d) \tag{17}$$

The random error in the prediction plane can be expressed as follows [26]:

$$\sigma^2(\hat{p}_z(m,n)) = \Delta^4\sum_m\sum_n \sigma^2(\hat{p}_H(m',n'))|h_{ZH}(m-m',n-n'+qN)|^2 \tag{18}$$

where

$$\sigma^2(\hat{p}_H(m,n)) = \sigma_1^2|a_1(m',n')|^2 + \sigma_2^2|a_2(m',n')|^2 \tag{19}$$

The error due to the position mismatch is given by

$$\sigma_1^2|a_1(m',n')|^2 + \sigma_2^2|a_2(m',n')|^2 = \sigma_x^2|V_x(m',n')|^2 + \sigma_y^2|V_y(m',n')|^2 \tag{20}$$

The error due to the sensor mismatch is given by

$$\sigma_1^2|a_1(m',n')|^2 + \sigma_2^2|a_2(m',n')|^2 = \sigma_m^2|p_H(m',n')|^2 + \sigma_\phi^2|\mathrm{j}p_H(m',n')|^2 \tag{21}$$

where p_H is the pressure in the hologram plane, $V_x(m',n')$ the slope in the x direction, $V_y(m',n')$ the slope in the y direction, σ_x the variance of ε_x, ε_x the position error in the x direction, σ_y the variance of ε_y, ε_y the position error in the y direction, σ_m the variance of ε_a, ε_a the magnitude error, σ_ϕ the variance of ε_ϕ and ε_ϕ the phase error.

The amplification ratio R'_σ of the random error, which takes filtering into account, expresses the relation between the energies of the random errors in the hologram and prediction planes, g_H and g_Z, respectively, as follows:

$$g_Z = g_H \times R'_\sigma \tag{22}$$

$$\begin{aligned}10\log_{10}R'_\sigma \approx{}& 24.9(d/\Delta z) - 5.92(kd) + 1.55(d/\Delta z)^2\\ &+ 5.07(d/\Delta z)(kd) - 0.25(kd)^2 + 20\log_{10}(\Delta h/\Delta z)\ \mathrm{dB}\end{aligned} \tag{23}$$

where the prediction spacing is $\Delta_Z = \pi/k'_{\max}$ and the measurement spacing is $\Delta_H = \pi/k_{\max}$.

3. Development

3.1. Experimental study using NAH

The test set-up used for the measurements is shown in Fig. 4. The set-up included a rod with holes in which four 1/4 in microphones were placed 1.5 cm apart. The rod was mounted on a robot that moved the linear array microphone beside the box. The materials of the multilayer structures used were 49×61 cm in size and were mounted in a window in a wooden box of dimensions $110.4\times69.9\times47.3$ cm. The wooden box was covered on the inside with a polyester fibre that had an average absorption coefficient of 0.6. The layers were allowed to settle to ensure that there were no air gaps between the layers and the sound-absorbing material. All of the panels were mounted with an elastic adhesive at the edge. The sampling

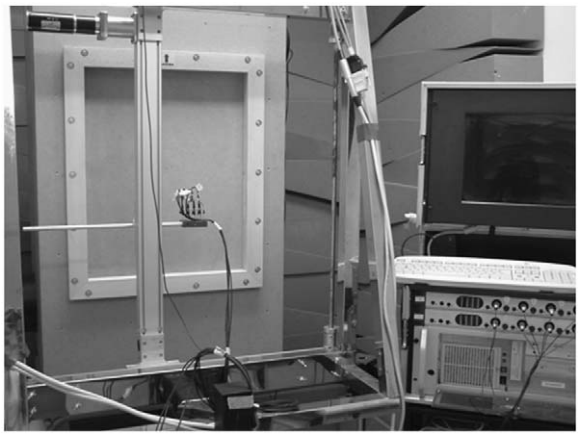

Fig. 4. Experimental setup and the robot with the array.

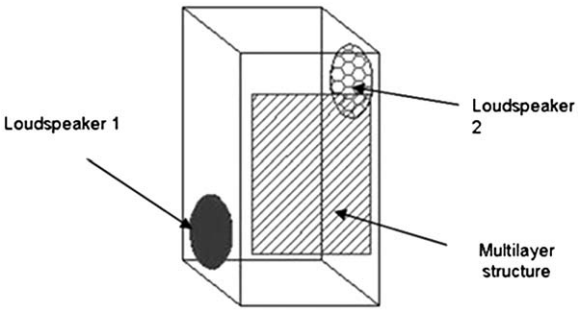

Fig. 5. Position of the speakers and multilayer structure.

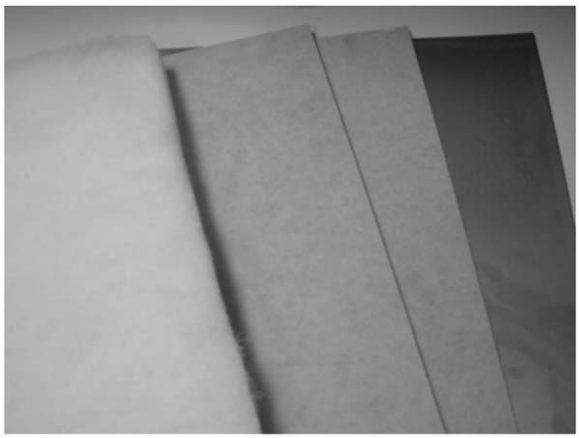

Fig. 6. Materials used in the study.

frequency was 44 100 Hz and the maximum frequency measured was 22 kHz. The size of the measurement array was increased until it was double that of the multilayer structure for the minimum frequency of 238 Hz. Two broadband speakers were located on each side of the box (Fig. 5) and the room was half-lined with sound-absorbing wedges [33].

A pulse of white noise 3 s in duration was generated by the speakers located inside the box and was maintained at the same intensity for all measurements. The noise generated inside the box was transmitted through the material of the box window and the response was recorded by the microphones over the measurement area and in the near field. A total of 1064 recordings were taken, distributed in a 28×38 matrix. The materials used in the study were analysed individually and in combination; they included a 1 mm steel sheet, 2.5 cm polyester wool plates and 3 and 5 mm boards made from a derivative of wood known as DM, which was formed from a very fine wood powder and had an isotropic behaviour (Fig. 6).

Measurements were taken at a distance of 2 cm from the window that contained the materials of interest. The data were then analysed using NAH to calculate the acoustic pressure and the vibration velocity on the surface of the material outside the window. The filter parameters were $k_c = 0.6k_{\max}$ and $\alpha = 0.2$.

The transmission loss from the interior to the exterior of the box was calculated according to the following equation [33,34]:

$$(L_S - L_R) = \mathrm{TL} \tag{24}$$

where L_S is the sound pressure level (measured in dB) in the source region, i.e., inside the box and L_R the sound pressure level in the receiver zone, i.e., on the material surface. Diffusers were placed inside the box to enhance the homogeneity of the acoustic field. Resonance phenomena are really serious for low frequencies and in small rooms. Above a frequency that depends on V, the volume of the room, on A, the absorption and on S, the surface area of the walls of the room, the number of excited modes is such that the acoustic field appears homogeneous and diffuse. Below this frequency, the modes are more spaced and they are perceived subjectively, giving rise to an acoustic field with heterogeneities. This frequency is known as the Schroeder frequency and is defined as the frequency where the modes start bunching so closely together that they no are longer seen as resonance peaks [7]. This frequency can be calculated from Eq. (25) below. In our particular case, this frequency was 460 Hz.

$$f_{\min} \approx c\frac{4}{\sqrt{[]\pi A}} - \frac{S}{16V} \tag{25}$$

An error in the measurement associated with the size of the panel and the effect of the window exists. Some authors include these effects within the total loss factor, so that in the model, the loss factor has contributions from the internal loss factor of the material, the loss factor associated with the conditions at the edge (which is reduced here with elastic elements) and the loss factor associated with the radiation efficiency [29]. In our case, the plates were thin and light and we know that their own resonances, associated with the wavenumber in the material and the dimensions, produced changes in the global loss factor. There is a discussion of this in the book by Cremer and Müller [29]. Nevertheless, this always happens in this type of model; it is something that is assumed as valid by many authors and whose effect is reduced when a constant value of the loss factor is obtained.

A sampling test of 30 measurements was performed with a microphone inside the box to estimate L_S. The data were averaged, yielding a dispersion of less than 2 percent; this result means that three measurements would have sufficed, but we decided to average the 30 measurements and then assume a uniform acoustic field. Octave bands were used to display the TL; the results are shown in Fig. 7. For all frequency ranges, higher values of TL were recorded for the multilayer structures than for the individual materials (5 mm wooden board and steel). A difference between '5 mm wood+wool+steel' and '5 mm wood+steel' was observed only in the frequency range within which the wool absorbed energy, i.e., at high sound frequencies; in this range, three-layered structures possessed a higher TL than two-layered systems. With respect to the TL of the individual materials, the TL for steel was about 5 dB more than that for 5 mm of wood. These data were used as input data in the inverse method.

The errors associated with the measured transmission loss can be calculated from the equation

$$\left|\frac{\partial \mathrm{TL}}{\mathrm{TL}}\right| = \left|\frac{\partial L_S}{L_S}\right| + \left|\frac{\partial L_R}{L_R}\right| \tag{26}$$

L_S has a small error because the number of measurements is high, 30 measurements. L_R has errors associated with the NAH measurements. The errors associated with this procedure depend strongly on the NAH measurements. We have evaluated the random error due to sensor and position mismatch in the planar acoustic holography measurements for a 5 mm wood+wool+steel multilayer [26]. The bias error can be regarded as negligible. The random error is significant in a backward prediction. The random error in the prediction plane was obtained for three measurement events. We studied the

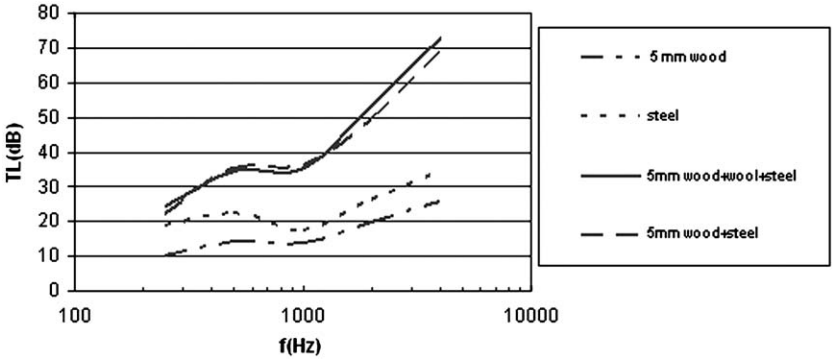

Fig. 7. Transmission loss obtained with NAH.

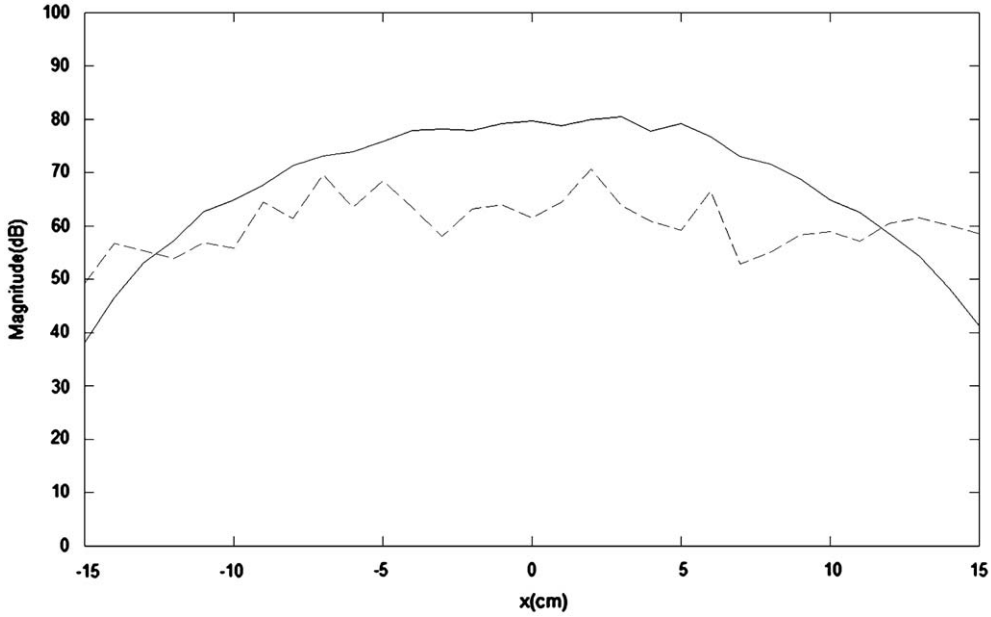

Fig. 8. Random error due to position mismatch.

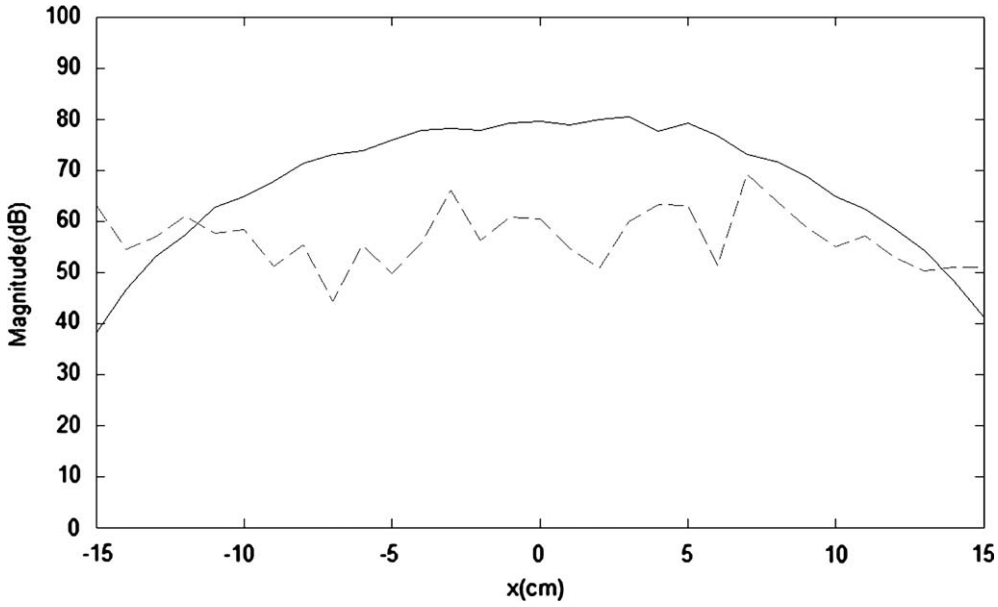

Fig. 9. Random error due to sensor mismatch.

spatial distribution of the random error in the prediction plane. The results for the random error due to position mismatch at 1 kHz are shown in Fig. 8 and those for the random error due to sensor mismatch are shown in Fig. 9. These figures show the magnitude of the pressure at the $y = 0$ line obtained by averaging the three measurement events and the random errors after wavenumber filtering ($10\log_{10}\sigma^2$) are also plotted. The random errors due to sensor and position mismatch have different shapes. In terms of their energies, the modified amplification ratio of the random error R'_σ between the random-error energies in the hologram and prediction planes is 12.7 dB.

3.2. Application of the inverse method

This section presents an inverse method, based on an SFT, for modelling the TL in multilayer structures using real-time measurements. The approach uses numerical methods to adjust the variables that define the layers in the system. The

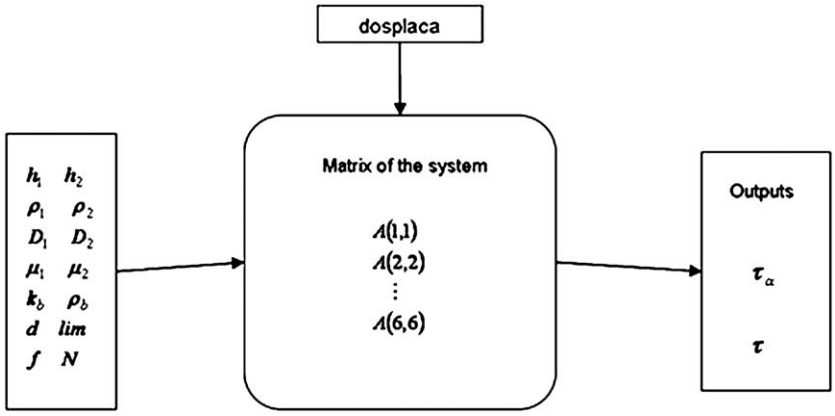

Fig. 10. Dosplaca software for the calculation of TL.

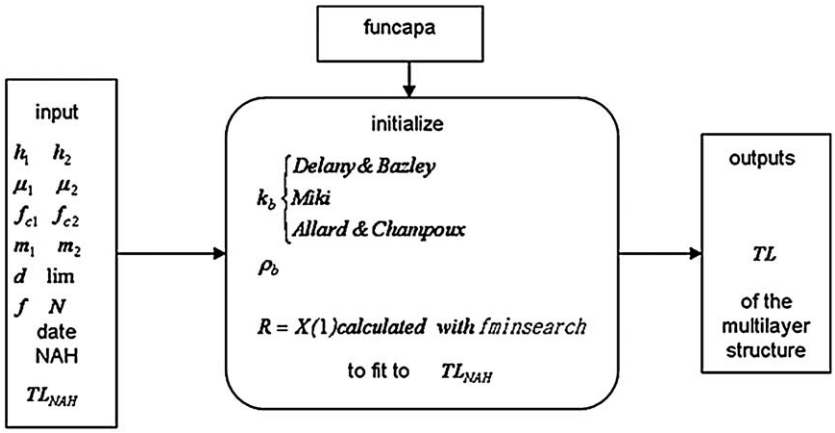

Fig. 11. Funcapa software adjust flow resistance.

results are then compared with those obtained using the Ookura and Saito model, which also predicts the TL in multilayer structures using values obtained via the inverse method and experimental results obtained using NAH as input parameters for the layers. Prediction models can also be used to simulate the acoustic behaviour of multilayer structures based on the acoustic characteristics that define each component element. For sound-impervious materials, these characteristics are the surface density, critical frequency and loss factor. For sound-absorbing materials, the flow resistance is used as input data.

Based on NAH measurements of the steel sheet and wooden board, various computer programmes were developed to calculate the mass per unit surface area, the critical frequency and the loss factor, following a procedure described in previous studies [35,36]. A MATLAB© function named 'fminsearch' was used to minimize the error. In this procedure, as described in the above publications, an error function is reconstructed that causes the model values to converge to the real-time measurement data. This procedure generates well-fitted parameters for impervious layers. Next, based on the available data for the '5 mm wood+polyester wool+steel' multilayer structure, the method described in [15] was applied. This method is a numerical procedure that was used to obtain the flow resistance of wool placed within a double partition. A MATLAB© function was also used to obtain this parameter with minimum error.

Although the flow resistance (Rayls/m) can be estimated using other methods, we decided to use the above technique because it is easy to implement and because it calculates the overall response of the system without the need to separate the two layers that form the polyester wool material. The algorithms used in this analysis are described below in greater detail. Fig. 10 shows the algorithm that was developed for the calculation of the TL (dB) of multilayer structures using the SFT model. The input data for the plates and sound-absorbing material are known: h_1 and h_2 are the plate thicknesses (m), ρ_1 and ρ_2 are the plate densities (kg/m^3), D_1 and D_2 are the flexural stiffnesses (N m), μ_1 and μ_2 are the loss factors of the plates (dimensionless), lim represents the limit angle (°), N is the number of steps of the angular integration, d is the thickness of the chamber (m), k_b is the complex wavenumber (rad/m) and ρ_b is the complex density of the sound-absorbing material (kg/m^3). By calculating the matrix of the system based on an SFT, we obtain as output data τ_α (the transmission coefficient, obtained as a function of the incidence angle) and τ (the dimensionless transmission coefficient, for a diffuse field).

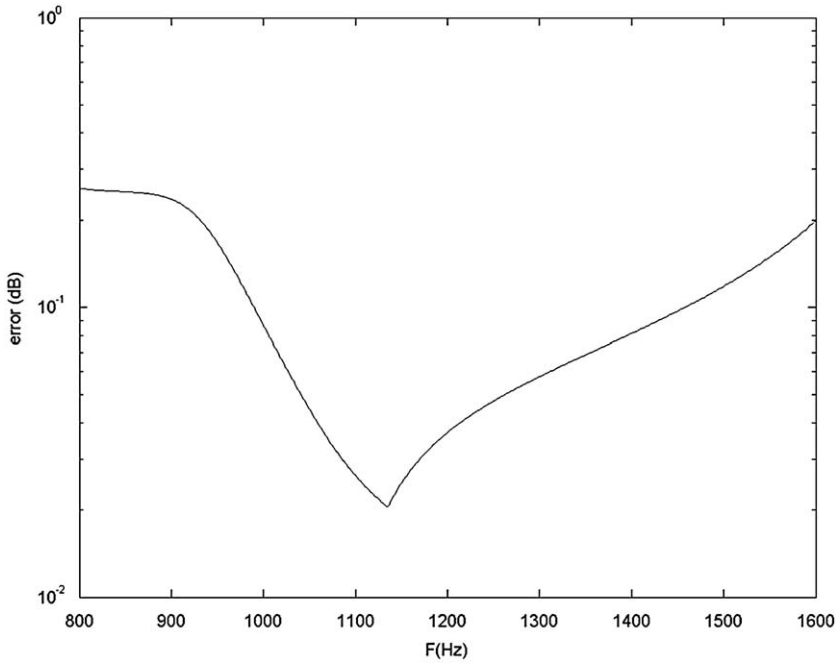

Fig. 12. Error function (dB) of f_c of a single wood plate.

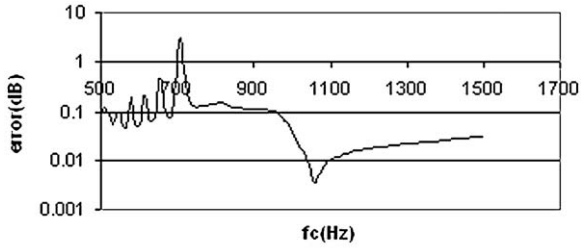

Fig. 13. Error function (dB) of f_c of multilayer structure.

Fig. 11 shows the Funcapa software package, which, given the parameters of the plates, adjusts the flow resistance of the sound-absorbing material such that the resulting TL fits the TL obtained via NAH. Funcapa calculates the flow resistance using as input data the critical frequencies f_{c1} and f_{c2} of the plates, the surface densities m_1 and m_2 of the plates and the TL obtained using NAH. The following MATLAB© function is then run:

$$y = \text{fminsearch}(\text{'funcapa'}, X) \tag{27}$$

where y is the minimum value of the error function, calculated in Funcapa using the criteria expressed by the function 'fminsearch', with respect to the difference between the experimental measurements and the theoretical value of the TL. Funcapa calculates the error at each iteration, which is retained in order to represent it. X is the value that starts the function and yields a local minimum y, close to X; the function 'funcapa' accepts the input y and returns a scalar function value. The function 'fminsearch' is based on the Nelder–Mead algorithm. This function minimizes a nonlinear function of n real variables using only function values, with no additional data [37]. The function minimizes the error function $\varepsilon = \sum_{i=1}^{n}(\mathrm{TL}_i - \hat{\mathrm{TL}}_i)^2$ calculated in Funcapa and generates an optimal value that ensures a better fit of the TL to the NAH values. All of the other parameters for the plates, such as the loss factors and critical frequencies, can be evaluated following the same procedure to obtain a better fit of the TL to the NAH values. The algorithm identifies the parameters for each individual frequency and then calculates the average in 1/3 octave bands.

We first considered the simple case of a 5 mm wooden plate. Using the measurements of the TL obtained using NAH and assuming a loss factor for the wood of 0.02, the range of the critical frequency was constrained to between 800 and 1600 Hz; these values are typical for tables made from this type of wood. Fig. 12 displays the error (measured in dB) obtained for the critical frequency of this simple wooden plate; the critical frequency was approximately 1140 Hz. Next, a

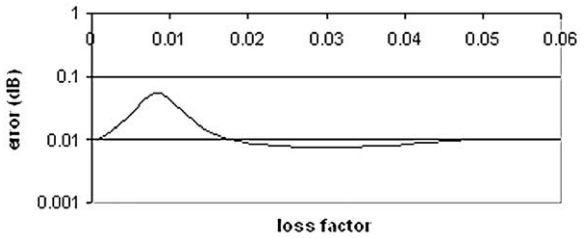

Fig. 14. Error function (dB) vs loss factor of multilayer structure.

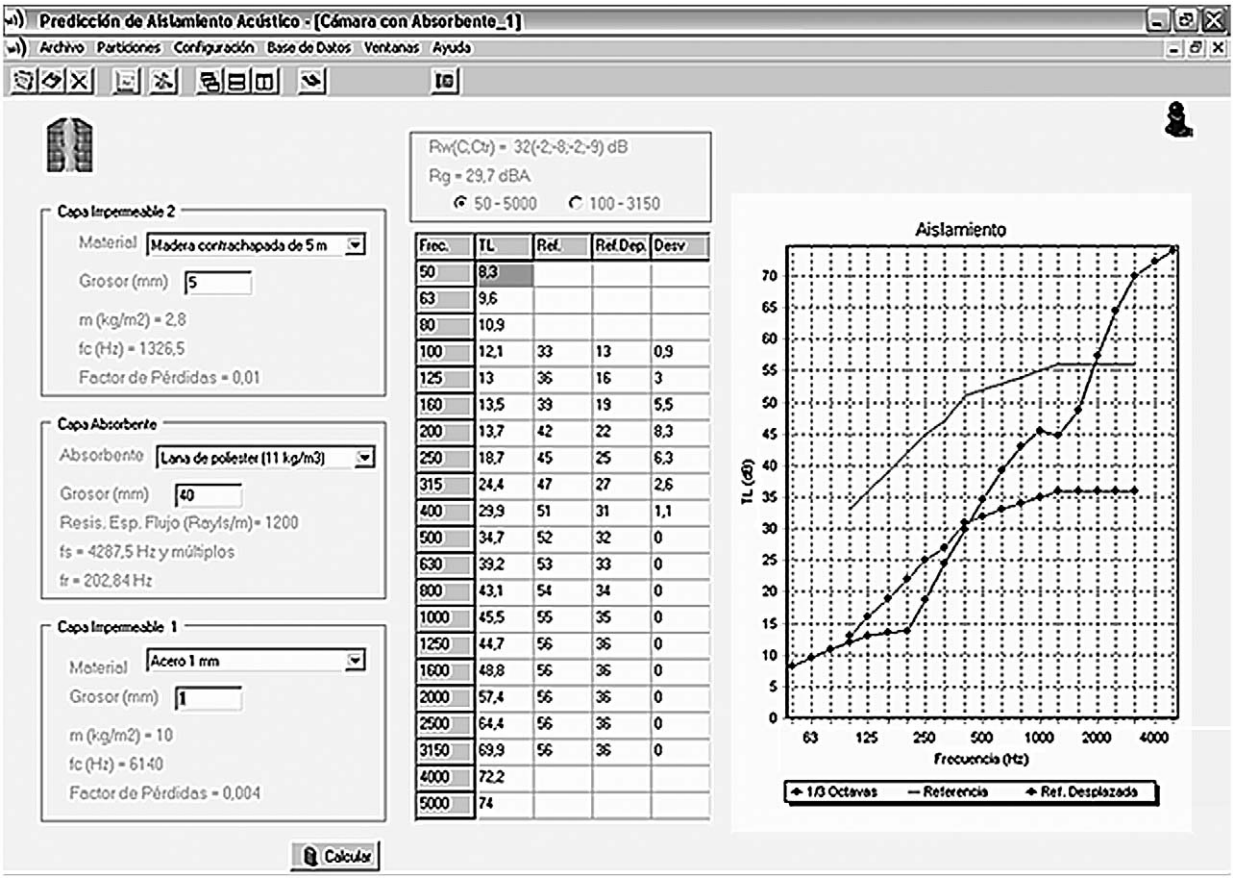

Fig. 15. Aisla 3.0 software.

multilayer structure was evaluated, where we considered a range of values of 0–0.05 for the loss factor and a critical frequency ranging from 500 to 1500 Hz for the layers. The errors were obtained where the minimum error yields the approximate value of the critical frequency and the loss factor of the wooden layers.

Fig. 13 shows the error (measured in dB) obtained at the critical frequency of the multilayer structure. Note that the minimum error gives the optimal frequency for fitting, approximately 1070–1090 Hz. Fig. 14 shows the loss factor, which has an optimal value of approximately 0.020–0.032.

For a single layer, the critical frequency obtained was 1140 Hz, while for the multilayer structure, the value was 1070–1090 Hz. The difference of about 50–70 Hz represents an error of 5–7 percent. This deviation may reflect the fixation conditions in the two different cases.

To enable comparison with the results of other prediction models for acoustic insulation in multilayer structures, we used the Aisla 3.0 software package [38] to calculate the TL according to the Ookura and Saito model [1] (Fig. 15). In this case, only the materials and sound-absorbing material of the multilayer structure were selected. When a material and thickness are selected, the computer program retrieves from its database the critical frequency, surface density and loss factor. The program also provides the flow resistance of the sound-absorbing material for the given thickness.

Table 1
TL (dB) calculated using NAH.

	f (Hz)	250	500	1000	2000	4000
TL (dB)	Steel	19	23	18	27	34
NAH	5 mm wood	11	15	14	20	26

Table 2
Specifications of the analysed materials.

	Steel	Wood
Thickness (mm)	1	5
Surface density (kg/m^2)	10	3.8
Critical frequency (Hz)	12 500	1000
Loss factor	0.004	0.024

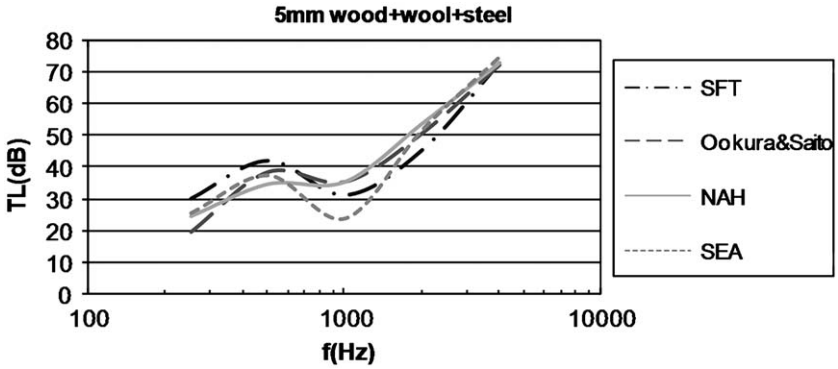

Fig. 16. Comparison of models for 5 mm wood+wool+steel.

The TL was calculated using NAH as described in the previous section. The TL values for the 5 mm wood and 1 mm steel plates obtained from the experimental measurements were used as input data for the SFT model (Table 1); the inverse method was then used to calculate the specific data for each material (Table 2).

The measured value of the critical frequency of the steel plate was 12 500 Hz. On the basis of this result, we considered that as the critical frequency of the steel plate was outside the measurement range, the model fitted all of the variables, but the elastic constants did not give real information because there was not sufficient information in the measurements. If we did not use these results, there would be no significant effect on other predictions either, since all of the other predictions applied to the same range of frequency. Therefore, the usefulness of the method is limited to materials with a critical frequency within the measurement range. This can be observed in the measurements, since the critical frequency corresponds to a diminution of the isolation.

The data obtained using the inverse method was used to calculate the TL for various multilayer structures. The input data for the model of the absorbing material was the flow resistance, which in the present case was 1200 Rayls/m.

Figs. 16 and 17 show the TL for the '5 mm wood+wool+steel' multilayer structure and '3 mm wood+wool+steel' multilayer structure, respectively, obtained using the Trochidis and Kalaroutis (based on an SFT), Ookura and Saito (Aisla 3.0) and SEA models, as well as the TL obtained using NAH. All of the models and the NAH technique yield similar trends for the TL.

Our measurements were carried out using a fast Fourier transform. However, the commercial software package that we used gives values in octave bands; that is to say, from a set of discrete frequencies in each octave band, energy averages are obtained and an average represents all of the band. For example, the octave band for 1 kHz groups together frequencies from 707 to 1414 Hz. Another example is shown in Fig. 18. This graph shows the effect of the bands and the way in which the values change depending on which band is used. It can be observed that the tendency is the same, but the values are different. In our case Aisla was chosen in order for us to be able to compare the tendency in our results with the results of a commercial software package, but the values do not have to agree exactly, because our measurement was based on a fast Fourier transform.

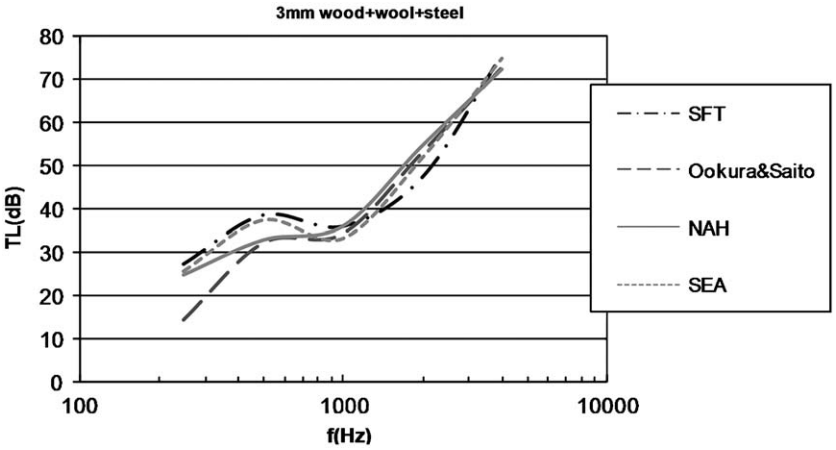

Fig. 17. Comparison of models for 3 mm wood+wool+steel.

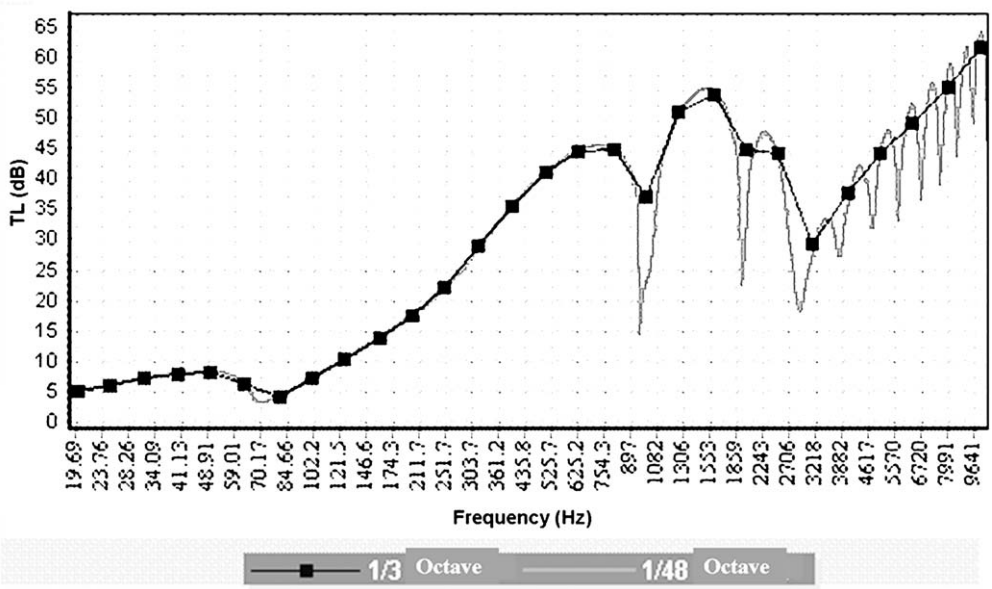

Fig. 18. Effect of the bands in the TL of a multilayer structure.

The conditions of connection between the components of the multilayer system act to increase the loss factor, vary the elastic parameters to a small degree and reduce the TL of the laboratory measurements relative to *in situ* measurements [39,40].

4. Conclusions

The inverse method employed in the present study provides good results in terms of determining the unknown parameters for the layers when the Trochidis and Kalaroutis prediction model for the transmission loss in multilayer structures is used and experimental data obtained by NAH is used as input data. The results obtained by our method were compared with results obtained using the Ookura and Saito prediction model and the SEA model. The results obtained were satisfactory for the range of sound frequencies analysed in the study, as limited by the constraints of the experimental set-up.

Estimates of the effectiveness of acoustic insulation can be complemented by and adjusted with additional experimental measurements obtained using test set-ups that resemble real environments; such an approach does not require real-time measurements. We have analysed the effect of measurement errors on the procedure. The most

significant errors are the random errors due to sensor and position mismatch and can be amplified significantly in the backward prediction.

Acknowledgements

This work was supported by the Ministry of Education and Science (BIA2007-68098-C02-01 and BIA2007-68098-CO2-02), by Conselleria de Empresa, Universidad y Ciencia (APOSTD/2007/112) and by Conselleria de Educación de la Generalitat Valenciana (GVPRE/2008/115).

References

[1] K. Ookura, Y. Saito, Transmission loss of multiple panels containing sound absorbing materials in a random incidence field, *International Conference on Noise Control Engineering*, *Inter-Noise 78*, San Francisco, CA, May 1978.
[2] A. Trochidis, A. Kalaroutis, Sound transmission through double partitions with cavity absorption, *Journal of Sound and Vibration* 107 (1986) 321.
[3] M. Bruneau, *Manual d'Acoustique fondamentale*, Edition Hermès, Paris, 1998.
[4] W. Lauriks, P. Mees, J.F. Allard, The acoustic transmission through layered systems, *Journal of Sound and Vibration* 155 (1) (1992) 125–132.
[5] A.J. Price, M.J. Crocker, Sound transmission through double panels using statistical energy analysis, *Journal of the Acoustical Society of America* 47 (3) (1969) 683–693.
[6] R. Panneton, N. Atalla, Numerical prediction of sound transmission through finite multilayer systems with poroelastic materials, *Journal of the Acoustical Society of America* 100 (1) (1996) 346–354.
[7] R.J.M. Craik, R.S. Smith, Sound transmission through double leaf lightweight partitions—part I: airborne sound, *Applied Acoustics* 61 (2000) 223–245.
[8] M. Garai, F. Pompoli, Definition and first validation of a new mathematical model of polyester fibre materials, *Forum Acusticum*, Seville, 2004.
[9] J.F. Allard, Y. Champoux, New empirical equations for sound propagation in rigid frame fibrous materials, *Journal of the Acoustical Society of America* 91 (6) (1992) 3346–3353.
[10] K.U. Ingard, T.A. Dear, Measurement of acoustic flow resistance, *Journal of Sound and Vibration* 103 (4) (1985) 567–572.
[11] ISO 10534-1, Acoustics—determination of sound absorption coefficient and impedance in impedance tubes—part 1: method using standing wave ratio (1996), part 2: transfer-function method (1998).
[12] M.E. Delany, E.N. Bazley, Acoustical properties of fibrous absorbent materials, *Applied Acoustics* 3 (1970) 105–116.
[13] Y. Miki, Acoustical properties of porous materials—modifications of Delany–Bazley models, *Journal of the Acoustical Society of Japan (E)* 11 (1) (1990) 19–24.
[14] L.E. Kinsler, A.R. Frey, A.B. Coppenns, J.V. Sanders, *Fundamentals of Acoustics*, Wiley, New York, 2000.
[15] J. Alba, J. Ramis, Modeling of impervious layers from measurements of the sound reduction index, *Applied Acoustics* 64 (2003) 385.
[16] Y. Shi, H. Sol, H. Hua, Material parameter identification of sandwich beams by inverse method, *Journal of Sound and Vibration* 290 (2006) 1234–1255.
[17] J. Alba, J. Ramis, V. Sanchez-Morcillo, Improvement of the prediction of transmission loss of double partitions with cavity absorption by minimization techniques, *Journal of Sound and Vibration* 273 (2004) 793–804.
[18] E. Dascotte, Identification of random material properties using a mixed deterministic–probabilistic method, *International Conference on Noise & Vibration Engineering*, 2004.
[19] D. Szeliga, J. Gawad, M. Pietrzyk, Parameters identification of material models based on the inverse analysis, *International Journal of Applied Mathematics and Computer Science* 14 (4) (2004) 549–556.
[20] T. Lauwagie, H. Sol, G. Roebben, W. Heylen, Y. Shi, Validation of the Resonalyser method: an inverse method for material identification, *International Conference on Noise & Vibration Engineering*, 2002.
[21] J.D. Maynard, E.G. Williams, Y. Lee, Nearfield acoustic holography: I. Theory of generalized holography and the development of NAH, *Journal of the Acoustical Society of America* 78 (4) (1985) 1395–1413.
[22] E.G. Williams, H.D. Dardy, Nearfield acoustical holography using an underwater, automated scanner, *Journal of the Acoustical Society of America* 78 (2) (1985) 789–798.
[23] E.G. Williams, *Fourier Acoustics, Sound Radiation and Nearfield Acoustical Holography*, Academic Press, San Diego, 1999.
[24] E.G. Williams, Numerical evaluation of the radiation from unbaffled, finite plates using FFT, *Journal of the Acoustical Society of America* 74 (1) (1983) 343–347.
[25] E.G. Williams, Intensity vector field mapping with nearfield holography, *International Congress on Recent Developments in Acoustic Intensity Measurements*, CETIM, France, 1981.
[26] K.-U. Nam, Y.-H. Kim, Errors due to sensor and position mismatch in planar acoustic holography, *Journal of the Acoustical Society of America* 106 (4) (1999) 1655–1665.
[27] A. Martínez, Identificación de tensiones iniciales en un macizo rocoso a partir de medidas de presión de agua en las excavaciones de túneles, Thesis, Universidad Politécnica de Cataluña, 2003.
[28] E.G. Williams, J.D. Maynard, Numerical evaluation of the Rayleigh integral for planar radiators using the FFT, *Journal of the Acoustical Society of America* 72 (6) (1982) 2020–2030.
[29] L. Cremer, H. Müller, *Principles and Applications of Room Acoustics*, Applied Science Publishers, London, 1982, p. 238.
[30] W.A. Veronesi, J.D. Maynard, Nearfield acoustic holography (NAH) II. Holographic reconstruction algorithms and computer implementation, *Journal of the Acoustical Society of America* 81 (5) (1987) 1307–1322.
[31] J.D. Maynard, E.G. Williams, Nearfield acoustic holography, a new technique for noise radiation measurement, *Proceedings of the National Conference on Noise Control Engineering*, *Noise-Con 81*; North Carolina State University, Raleigh, NC, June 8–10, 1981.
[32] T.H. Burns, Measurement and Visualization of Instantaneous Power Flow in Steady-State Acoustic Fields, Thesis, UMI Dissertation Services, 1995.
[33] E. Escuder, Estudio del comportamiento acústico de estructuras multicapa mediante NAH, Doctoral Thesis, Universidad Politécnica de Valencia, 2005.
[34] C.M. Harris, *Manual de medidas acústicas y control del ruido*, McGraw-Hill, Madrid, 1995.
[35] J. Alba, J. Ramis, J. Llinares, Caracterización de capas impermeables a partir de medidas de aislamiento, *Revista de Acústica* XXXII (2001) 1 y 2.
[36] J. Alba, J. Ramis, V. Espinosa, V. Sánchez-Morcillo, Radiación acústica por superficies planas: aplicación a altavoces, *Revista Internacional de Métodos Numéricos para Cálculo y Diseño en Ingeniería* 19 (1) (2003) 65–74.
[37] J.C. Lagarias, J.A. Reeds, M.H. Wright, P.E. Wright, Convergence properties of the Nelder–Mead simplex method in low dimensions, *SIAM Journal on Control and Optimization* 9 (19) (1998) 112–147.
[38] J. Alba, Algoritmos de modelado de particiones multicapa para la predicción de su aislamiento acústico a ruido aéreo, Doctoral Thesis, Universidad Politécnica de Valencia, 2000.
[39] UNE-EN 12354-1, Building acoustics. Estimation of acoustic performance of buildings from the performance of elements—part 1: airborne sound insulation between rooms, 2000.
[40] R. Josse, *Acoustics in Construction*, Gustavo Gili, Barcelona, 1975.